Structural Evolution of Smaller Gold Nanocrystals: The Truncated Decahedral Motif

Charles L. Cleveland,[1] Uzi Landman,[1] Thomas G. Schaaff,[2] Marat N. Shafigullin,[2]
Peter W. Stephens,[3,4] and Robert L. Whetten[1,2]

[1]School of Physics, Georgia Institute of Technology, Atlanta, Georgia 30332
[2]School of Chemistry, Georgia Institute of Technology, Atlanta, Georgia 30332
[3]Department of Physics, State University of New York, Stony Brook, New York 11794
[4]National Synchrotron Light Source, Brookhaven National Laboratory, Upton, New York 11973

Atomistic modeling of energetics and structures, coupled with x-ray powder diffraction analyses of size-separated passivated gold nanocrystals in the $1-2$ nm size range, shows preferential formation of a stable sequence of three cluster sizes, all with a truncated-decahedral motif.   [S0031-9007(97)03951-3]

It is commonly expected, and often observed, that the structures (and properties) of finite-size materials aggregates (clusters) differ from those of the bulk. However, determination of specific cluster structures, identification of structural motifs, and elucidation of size-evolutionary patterns, which are central issues in cluster and nano-science, remain vexing problems [1]. Here we show that the structural size evolution in gold may be described as a sequence of transitions: (i) from specific "molecular" structures, at the extremely small size range, with equivalent cluster diameter $d_{eq} \leq 1$ nm (<40 atoms), to (ii) ordered "noncrystallographic" (decahedral) structures (here we use this term for motifs which do not occur in bulk crystals, e.g., fivefold symmetric ones) at larger sizes, and then culminating with sizes with $d_{eq} > 2$ nm (~ 250 atoms), in (iii) crystallites of bulk lattice structure (fcc) with specific faceted morphologies (i.e., truncated octahedra, variants thereof, and their twins). Since the first regime has been commonly discussed in the cluster literature [2] and the "convergence" to the bulk structure for large clusters (iii) was described by us in some detail elsewhere [3(a),3(b)], we focus here on the intermediate regime (ii) which is also the least "intuitive" and harder to resolve.

While previous studies using high-resolution electron microscopy (HREM) on supported larger ($d_{eq} \geq 3$ nm) gold crystallites yielded valuable information [4], the application of the method to studies of smaller clusters is limited by image-contrast, momentum-transfer, and beam-induced mobility considerations. Similarly, extraction of structural information from mass-selected cluster beams [5] encounters severe difficulties because abundances are controlled by evaporation, requiring for Au clusters temperatures above melting, as well as by electronic shell-structure effects [6] which heavily obscure spectroscopic signatures of atomic structure in the pertinent size-range, and time-scale limitations which complicate the assessment of structural metastability of various isomeric forms. Furthermore, single-crystal x-ray diffraction (XRD) has so far been applied only to crystals of gold cluster compounds made of small highly charged cores (the largest being Au_{39}^{+7}[7]) bound to complex ligands and counte-

rions. In conjunction with the limited systematic experimental information in the $1-2$ nm size range, theoretical investigations have variously predicted differing crystallographic [8], noncrystallographic [9], amorphous [10], and melted or quasimelted forms [4(a)], resulting in a lively debate with no consensus or confirmed resolution.

Our approach is based on predictions and insights obtained through exploration of the atomistic energetics and structures of Au_N ($50 \leq N \leq 5000$) clusters which led to the identification [3(a),3(b)] of energetically optimal discrete cluster-size sequences, each associated with a structural motif, in juxtaposition with the preparation and isolation of macroscopic amounts of well-fractionated (by size) stable gold nanocrystallites (in solution, and as powders, films, and superlattices [3]) on which powder XRD, and other measurements, have been performed [3(a),3(b)].

In the extensive structural survey, performed through energy minimization of atomistic models with many-body embedded-atom interactions [3(a),3(b)], and aided by a cluster genetic algorithm (CGA) [11], we included a broad range of structural forms, guided by actual observations (mainly, HREM and XRD) as well as by past experience [12] and the CGA. These include (i) fcc structures with various morphologies (cube-octahedra (CO), octahedra (Oh), truncated octahedra (TO, TO$^{\pm}$) [3]), and their twinned variants; (ii) icosahedral (Ih) and capped-Ih (c-Ih) structures; (iii) hexagonally close-packed (hcp) structures; (iv) pentagonal decahedral (Dh) arrangements and their variants, i.e., ino-Dh (i-Dh) (see description in Ref. [12]), and Marks-Dh (m-Dh), where reentrant (111) facets are introduced via a modified-Wulff construction to optimize the clusters' energetic stability through a balance between surface and strain energy contributions [13]; and (v) partially disordered clusters obtained through molecular dynamics (MD) simulations at elevated temperatures.

Because of their discrete nature, atomistic models of various structural motifs and morphologies correspond to specific size (number of atoms) sequences. For example, the number of atoms in decahedral crystallites can be expressed as $N = 1/6\{30p^3 - 135p^2 + 207p - 102 + [5m^3 + (30p - 45)m^2 + (60(p^2 - 3p) + 136)m] +$

$n[15m^2 + (60p - 75)m + 3(10p^2 - 30p) + 66]\} - 1$, with m, n, and p as defined in Fig. 1 (inset). Examination of the energetics of the various structural motifs (Fig. 1) leads to the identification of the energy-optimal pattern ("magic number" sequence). This procedure predicts that m-Dh clusters and fcc TO clusters (and their TO^+ and twinned variants) form the dominant size sequence for Au_N. Furthermore, except in the very small size range, the Ih motif is found to be energetically noncompetitive (due to accumulated icosahedral strain which grows with volume [12]); fcc clusters with Oh and CO morphologies are also noncompetitive, with energies of the latter lying above the scale of the figure, and the competition between the fcc-TO motif and the Dh motif maintains throughout, with the Dh advantage somewhat diminishing for larger clusters (due to accumulated volume-dependent decahedral strain, which is smaller than the icosahedral strain [12]). In the size range of interest to us here, the lowest-energy cluster sequence is made of Au_{75}, Au_{101}, and Au_{146}, all belonging to the m-Dh motif, with the (m, n, p) indices as indicated in Fig. 1 (see circled stars). In this context it is interesting to note that a similar analysis performed earlier [12] for nickel clusters resulted in the predominance of icosahedral clusters up to $\sim$1500 atoms, indicating that the preferred structural forms are material specific.

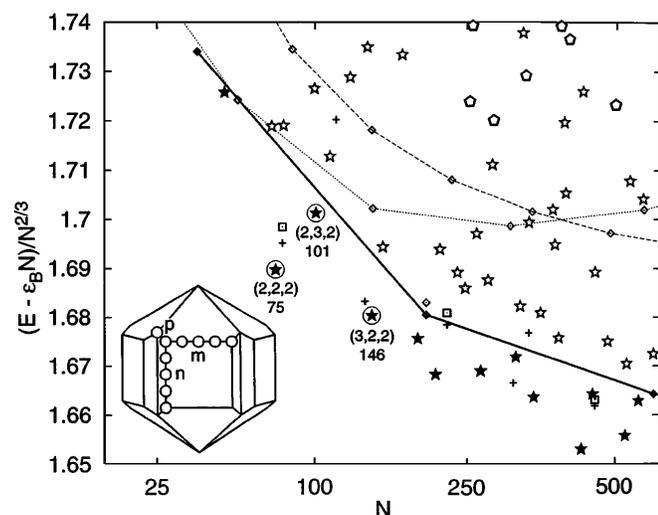The materials used in this study were prepared by making use of the fact that, in the controlled growth of a solid from atoms, the rate (kinetics) can be drastically reduced, or effectively halted, at certain levels of aggregation corresponding to the formation of structures of "singular" thermochemical stability, which thereby accumulate. This effect can be strongly enhanced by the action of a reverse process (e.g., etching), the presence of which can further establish a local equilibrium (energetics). If these structures are protected against casual (contact) coalescence by a mild passivating agent, they can be accumulated in macroscopic quantities to the virtual exclusion of other sizes and structures, reducing our task to resolving a handful of structures obtained with extreme high statistical significance.

In the present case, charge-neutral Au clusters were obtained by the controlled [14] decomposition of AuSR molecules (R is an n-alkyl group denoted below by C_n) in the presence of excess $RSSR$ molecules, which act as a weak passivant as well as etching agents. These methods have recently been described in full [14], including the observation that in the pertinent size range well-controlled growth can result in the essentially quantitative conversion of atomically dispersed gold into three discrete clusters, with core masses near $14k$, $22k$, and $28k$ ($k = 1000$ amu, or 5.08 Au atoms; i.e., expressed in terms of the number of atoms, these isolated fractions consist of thiol-passivated gold clusters with gold cores of $\sim$70, 110, and 140 atoms, respectively). The subsequent separation of these clusters by fractional crystallization from solution into purified fractions, each on the $0.01g$ scale, was monitored via mass spectrometry. The resulting materials can be handled as molecular substances, with well-defined solutions and crystalline phases, and can thus be characterized compositionally (e.g., to verify that there is an elemental Au core [3(a),14]).

The fractions that can always be identified in the mass spectra, whether in mixtures or as pure substances, are (i) the $14k$ Au compound, the smallest one obtained in every case in appreciable yield and essentially the exclusive one obtained under the most severely controlled growth conditions [14] [here, the SC_{18} variant has been separated from residual higher compounds (mainly the $22k$ one) at the $\sim$85% level]; (ii) the $28k$ Au compound, easily obtained in high yield and often nearly the exclusive product of growth under slightly less restrictive conditions than just mentioned; (iii) the $22k$ compound, never obtained in yields approaching the above ones and quite difficult to obtain in high purity from those in (i) and (ii); and (iv) a mixture of two or more compounds in the $34k-42k$ mass range. The mass-spectroscopic analysis, as well as other characterizations (e.g., optical absorption and high-resolution transmission electron microscopy), indicate that the separated fractions are molecularly defined substances [3(a),3(b),14], rather than a continuum of sizes (and structures).

Figure 2 shows XRD intensity patterns [$I(s)$ vs $s = 2\sin\theta/\lambda$], where 2θ is the scattering angle, $\lambda = 1.5405$ Å] for powder samples of each of the

FIG. 1. Energies of structurally optimized Au_N ($N \leq 520$) clusters plotted as $(E - \varepsilon_B N)/N^{2/3}$ vs N (on an $N^{1/3}$ scale), where $\varepsilon_B = 3.93$ eV is the cohesive energy of an atom in bulk Au. Various structural motifs are denoted as Oh (-- ◇ --), Ih ($\cdots$◇$\cdots$), TO (—◆—), t-TO (◇), To^+ (+), t-TO^+ (□), i-Dh (⬠), and m-Dh (☆), with the filled stars denoting m-Dh clusters in the enhanced stability region. The 75, 101, and 146 atom m-Dh clusters corresponding to the stable structural sequence (see Fig. 2) are denoted by ✪. The (m, n, p) indices of m-Dh are shown in the inset, for a (5,5,2) cluster.
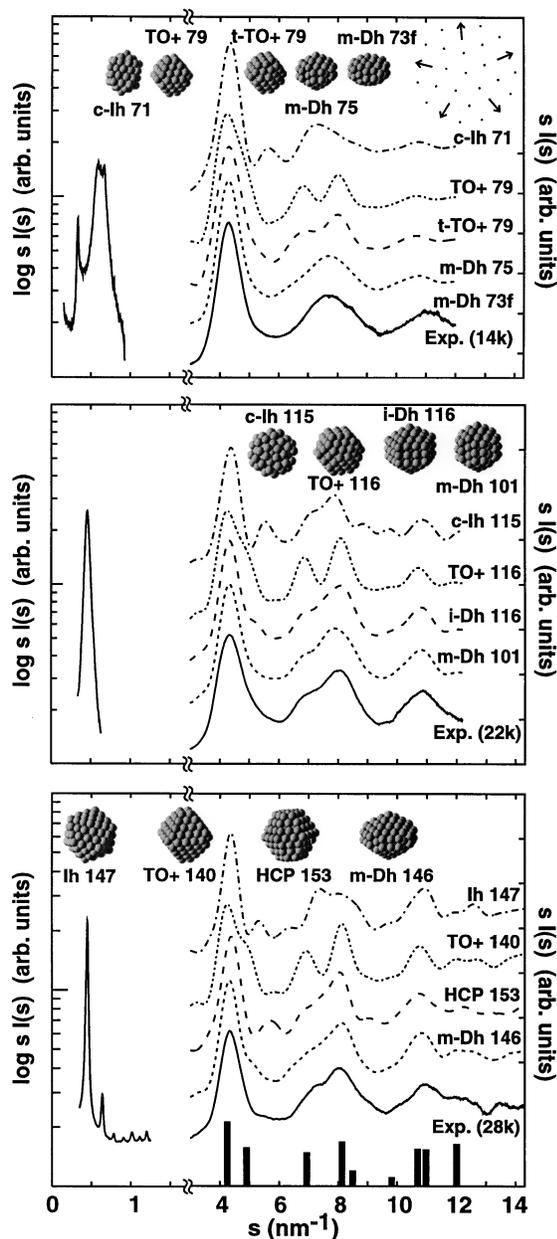
FIG. 2. Experimental (Exp.) and calculated powder XRD intensities (in arbitrary units) plotted vs s (in nm^{-1}). In each panel, measurements are given for the small s [left, $\log sI(s)$] and large s [right, $sI(s)$] for the well-separated $14k$, $22k$, and $28k$ nanocrystal gold samples (top to bottom panels). [Curiously, our XRD pattern for the $14k$ fraction is remarkably similar to that shown in Ref. [15] for the Au_{55} $[P(C_6H_5)_3]_{12}(Cl)_6$ cluster, commonly known as "Au_{55}," although its precise identity remains controversial [16].] In each case, the theoretical patterns (for large s) were calculated for various relaxed atomistic structural models (displaced vertically and denoted above each of the curves by the structural symbol followed by the number of atoms in the model, which is shown at the top of each panel) as described in the text. We note here that in comparing the measured intensities with those obtained for the theoretically predicted structures using the Debye formula [17], with exponential $\exp(-Bs^2/2)$ thermal damping and s-dependent atomic gold scattering factors, the *only* structural variation which was allowed from the predicted atomic coordinates is a uniform volume dilation (or compression) δ; other refinements such as shellwise dilations and/or axial dilation or compression did not improve the agreement in any significant manner. The best fits for the Dh clusters were obtained for $\delta \sim 3\%-4\%$, i.e., an outward displacement from the energy-optimized structures of the bare clusters, which themselves show a slight (an average $\sim -2\%$) contraction of the outer facets from their truncated-bulk positions. Such a small net expansion, as well as remaining discrepancies between the calculated and measured data, could be due to a combination of factors, such as interaction potentials, thermal expansion, and the effect of binding to the passivating molecules, as well as any residual imperfections in the size separation. Superior agreement is obtained for the 75, 101, and 146 atom m-Dh (circled filled stars in Fig. 1), with thermal damping factors B refined to 0.045, 0.020, 0.013 nm^2, respectively. The vertical bars on the axis of the bottom panel show the locations of reflections corresponding to bulk gold. In the top panel, we include a theoretically predicted curve (coinciding with the experimental data) for a 73 atom m-Dh (marked m-Dh 73f), where, starting from a relaxed m-Dh 75 cluster, a fit to the x-ray pattern was performed allowing *all* the atomic coordinates to vary freely, resulting in an oblate decahedral cluster, with the top and bottom vertex atoms removed. A top projected view indicates the positions of atoms in the m-Dh 73f cluster, and the arrows indicate the main displacements of atoms from their m-Dh 75 locations (in addition to those causing the axial compression). The ideally fitted m-Dh73f cluster is energetically much less stable than all other structures, illustrating the caution that must be exercised in comparing theoretical and experimental results.

well-separated ($14k$, $22k$, and $28k$) fractions. The stability of these materials is evidenced by the reproducibility of the XRD and other measurements for samples stored at room temperature for over one year, or for cooling the materials to 10 K and heating to 350 K for hours. For such molecular solids, the pattern at small s is dominated by a series of sharp peaks (superlattice Bragg peaks), which we have used, when possible, to corroborate the sizes obtained from the mass analysis and estimated density.

The intensity patterns observed at large s, which give information primarily about the internal atomic structure of the individual gold cores, exhibit maxima that, on first sight, may be associated with those of bulk fcc Au, yet the intensities are strongly altered and the detailed line shapes cannot be accounted for by simple finite-size approximations applied to the bulk structure. However, when analyzed using intensities from predicted structures, in conjunction with the size estimates, these line shapes can be used very effectively to exclude most of the plausible packing types (as well as amorphous and liquidlike structures), and identify the most favorable one. Figure 2 shows just a small selection of the comparisons made between the measured and calculated XRD patterns, in order to illustrate this process of elimination. Even a cursory inspection of the results displayed in Fig. 2 allows

an unambiguous rejection of all structures, with the exception of the Dh motif (in particular the m-Dh) which consistently yields superior detailed agreement with the data. In any case, the smallness of the deviation from the predicted bare-cluster structures serves as an *a posteriori* confirmation of their merit, substantiating further this "first-principles" mode of structural analysis [18] and the high quality of materials on which the measurements were made.

The best agreement with the data, to the exclusion of alternative ones, corresponds to (2,2,2) m-Dh 75, (2,3,2) m-Dh 101, and (3,2,2) m-Dh 146 clusters (see Figs. 1 and 2), which are the smallest nontrivial ($m, n, p > 1$) Marks decahedra. In each case, the theoretical curve is not changed when the number of atoms is reduced by two, corresponding to the removal of the top and bottom vertex atoms of the m-Dh (see Fig. 2). This sequence of clusters coincides with the optimal-energy one in this size range (see Fig. 1), and is in very close correspondence with the mass-spectrometrically estimated core masses of the fractionated samples used in the XRD measurements.

We conclude that for gold the 1 nm $\leq d_{eq} \leq$ 2 nm size range is punctuated by the formation of a discrete sequence of primarily three cluster sizes which correspond well to the most stable ones in this range (see Fig. 1), all belonging to the truncated (Marks)-decahedral motif with the particular truncations described above. This analysis provides an energetic and structural explanation for the observed preferential formation of this discrete sequence of stable gold nanocrystallites in this range. While similar structures of larger metal particles have been discussed experimentally and theoretically [4,12,13,19], they have not been previously associated with a stable metal cluster sequence in this size range. Along with a resolution of the structural issue, we demonstrated the ability to obtain macroscopic quantities of highly size-separated nanometer-scale metal clusters in a refined state (i.e., neutral cores with "weak" passivation which does not seem to disrupt the metal nanocrystallite structure). These findings have broad implications for measurements of various size and structure sensitive physical properties (e.g., electronic quantized transport processes in individual particles and their superlattices, and spectroscopic characteristics [20]) which are the subject of current research efforts, with a potential application in optoelectronics, nanocircuits, and sensor technologies.

[1] See articles in *Clusters of Atoms and Molecules,* edited by H. Haberland, Springer Series in Chemical Physics Vols. 52 and 57 (Springer, Berlin, 1994).

[2] For a recent review, see D. M. P. Mingos, J. Chem. Soc. **5**, 561 (1996).

[3] (a) R. L. Whetten *et al.,* Adv. Mater. **5**, 428–433 (1996); *Chemical Physics of Fullerenes 5 and 10 Years Later,* edited by W. Andreoni (Kluwer, Dordrecht, 1996), pp. 475–490; (b) C. L. Cleveland *et al.,* Z. Phys. D **40**, 503 (1997); (c) W. D. Luedtke and U. Landman, J. Phys. Chem. **100**, 13 323 (1996).

[4] (a) For a comprehensive review, see L. D. Marks, Rep. Prog. Phys. **57**, 603–649 (1994); (b) D. Grozea and L. D. Marks (unpublished).

[5] T. P. Martin, Phys. Rep. **273**, 199–241 (1996).

[6] W. A. deHeer, Rev. Mod. Phys. **65**, 611–676 (1993).

[7] B. K. Teo, X. Shi, and H. Zhang, J. Am. Chem. Soc. **113**, 2743 (1992).

[8] See, for example, A. Pinto *et al.,* Phys. Rev. B **51**, 5315 (1995), and references therein; X. Yu and P. M. Duxbury, *ibid.* **52**, 2102 (1995); A. N. Patil *et al.,* Z. Phys. D **26**, 135 (1993).

[9] D. Haberlen *et al.,* J. Chem. Phys. **106**, 5189 (1997).

[10] F. Ercolessi, W. Andreoni, and E. Tosatti, Phys. Rev. Lett. **66**, 911 (1991); I. Garzon and A. Posada-Amarillas, Phys. Rev. B **54**, 11 796 (1996).

[11] M. D. Wolf and U. Landman (to be published).

[12] C. L. Cleveland and U. Landman, J. Chem. Phys. **94**, 7376 (1991).

[13] L. D. Marks, Philos. Mag. **49**, 81 (1984).

[14] M. M. Alvarez *et al.,* Chem. Phys. Lett. **266**, 91 (1997); T. G. Schaaff, M. N. Shafigullin, and R. L. Whetten, J. Chem. Phys. (to be published).

[15] W. Vogel, B. Rosner, and B. Tesche, J. Phys. Chem. **97**, 11 611 (1993).

[16] H. Weller, Adv. Mater. **7**, 94 (1996); for a review, see R. C. Thiel *et al.,* Struct. Bond. **81**, 1–39 (1993).

[17] A. Guinier, *Xray Diffraction* (Freeman, San Francisco, 1963).

[18] Our analysis, based on atomistic energy minimization, is essentially parameter free and should be contrasted with multiparameter data-fitting procedures using guessed structures including weighted distributions of cluster sizes with differing structural and morphological motifs (see, e.g., Ref. [15]).

[19] B. D. Hall *et al.,* Phys. Rev. B **43**, 3906 (1991).

[20] M. M. Alvarez *et al.,* J. Phys. Chem. **101**, 3706 (1997).